PROCEEDINGS OF SCIENCE

Implications from 3-dimensional modelling of gamma ray signatures in the Galactic Center

Julien Dörner,[a,b,*] **Julia Becker Tjus,**[a,b,c] **Paul-Simon Blomenkamp,**[b,d] **Horst Fichtner,**[a,b] **Anna Franckowiak,**[b,d] **Mario Hoerbe**[a,b] **and Memo Zaninger**[a,b]

[a] *Theoretical Physics IV, Plasma Astroparticle Physics, Faculty for Physics and Astronomy, Ruhr University Bochum, 44780 Bochum, Germany*

[b] *Ruhr Astroparticle and Plasma Physics Center (RAPP Center), Germany*

[c] *Department of Space, Earth and Environment, Chalmers University of Technology, 412 96 Gothenburg, Sweden*

[d] *Astronomical Institute, Faculty for Physics and Astronomy, Ruhr University Bochum, 44780 Bochum, Germany*

E-mail: jdo@tp4.rub.de

The Galactic Center (GC) region has been intensively studied in gamma rays in the past decades. Fermi LAT has discovered a GeV excess which is not fully understood, and the first detection of a *PeVatron* by H.E.S.S. indicates the existence of cosmic ray sources providing energies up to a PeV or higher. The emission of TeV gamma rays in the GC is affected by the source position and the distribution of the gas, photons and magnetic field within this region. For the first time we model the TeV emission in a realistic three-dimensional distribution of gas as well as photon fields and use a complex magnetic field comprising the large-scale field structure and small-scale imprints of molecular clouds as well as non-thermal filaments. Additionally, we test different anisotropies of the diffusion tensor defined by the ratio of the diffusion coefficients perpendicular and parallel to the local magnetic field direction. We compute a two-dimensional gamma ray distribution and compare it with *H.E.S.S.* measurements.

38th International Cosmic Ray Conference (ICRC2023)
26 July - 3 August, 2023
Nagoya, Japan

*Speaker

PoS(ICRC2023)584

1. Introduction

The Galactic Center is an extreme astrophysical environment. It has been intensively studied at different wavelengths over the last decades and provides a unique astrophysical laboratory. Radio observations of the CO and HI lines have been used to study the molecular and atomic hydrogen content in the central molecular zone (CMZ) [1, 2]. The observation of high energy (HE) and very high energy (VHE) γ-ray emission can give insights into the local sources and the transport process of charged cosmic rays in this region. In the HE range, Fermi LAT discovered a GeV excess which is not fully understood [3–5]. At the TeV - PeV energies, the High Energy Stereoscopic System (*H.E.S.S.*) observed a *PeVatron*, a cosmic-ray accelerator reaching energies up to PeV [6, 7]. Especially [7] report a spatially broad diffuse gamma ray emission up to several tens of TeV.

Until now most approaches to model the gamma ray emission of the CMZ are done in one dimension, although recent models [8] show the need for detailed 3D modelling of the CMZ to understand the origin of the diffuse gamma ray emission. In [8] the authors show the impact of a 3D gas distribution and the impact on the morphology of the diffuse emission.

The impact of the 3D magnetic field configuration has not been considered so far. From heliospheric observations, it is known for some time, that the diffusion of cosmic rays along and perpendicular to a magnetic field line is different [9, 10]. It has also been shown by first principle simulations of the diffusion coefficient [11–13] and is applied in Galactic CR modelling [13–15] Going beyond these approaches, this work investigates the impact of different assumptions about the 3d magnetic field and the anisotropy of the diffusion tensor, $\epsilon = \kappa_\perp / \kappa_\parallel$, in this work.

2. Galactic Center environment model

To build a realistic model of the gamma ray emission of the CMZ a detailed knowledge of the 3D structure is needed. We base our environment model on the work of [16].

The distribution of the molecular hydrogen (H_2) is described by diffuse inter-cloud component taken from [1], eleven molecular clouds and a more detailed structure for the central five parsec around SgrA* . The diffuse gas model, which is responsible for the diffuse gamma ray emission, shows a much thinner disc than the observed gamma ray emission (see Fig. 1). Therefore, we adjust the scale-height of the gas profile to $H = 30$ pc, which is the upper limit of the uncertainty discussed in [1]. A comparison between the original and modified gas profile can be seen in Fig. 1.

The magnetic field is modelled by a superposition of an inter-cloud component $\vec{B}_{\rm IC}$ and a contribution of the known molecular clouds $\vec{B}^{(i)}_{\rm MC}$ and non-thermal filaments $\vec{B}^{(i)}_{\rm NTF}$. The details can be found in [16].

3. Simulation setup

We solve the CR transport equation

$$\frac{\partial n}{\partial t} = \nabla \hat{\kappa} \nabla n + \frac{\partial}{\partial E}\left[\frac{\mathrm{d}E}{\mathrm{d}t} n\right] + S(\vec{r}, E, t) \tag{1}$$

for the CR differential number density $n(E)$ using CRPropa3.2 [17]. The energy loss term $\mathrm{d}E/\mathrm{d}t$ considers the inelastic interactions of CR protons with the gas following the parametrisation of the cross sections from [18] as implemented by [19].

3.1 CR diffusion

The spatial diffusion is described by the diffusion tensor $\hat{\kappa}$. In a local frame at a magnetic field line the diffusion tensor can be written as $\hat{\kappa} = \mathrm{diag}(\kappa_\perp, \kappa_\perp, \kappa_\parallel)$ assuming $\vec{B} = B\vec{e}_z$. In this work we fix the ratio $\epsilon = \kappa_\perp/\kappa_\parallel$ between the perpendicular and parallel diffusion coefficient. We test five different values $\epsilon \in \{10^{-3}, 10^{-2}, 10^{-1}, 0.3, 1.\}$.

We use the prediction from the quasi-linear theory in a Kolmogrov-like turbulence for the energy scaling of the diffusion coefficients and normalise the parallel one to the observed value at the location of the sun [20]. The parallel diffusion coefficient can be written as

$$\kappa_\parallel(E) = 6.1 \cdot 10^{28}\,\mathrm{cm^2\,s^{-1}} \cdot (E/4\,\mathrm{GeV})^{1/3} \quad . \tag{2}$$

3.2 CR sources

We simulate CR protons with energies between $1\,\mathrm{TeV} \leq E \leq 1\,\mathrm{PeV}$ with a flat energy distribution in logarithmic space, $dN/dE \sim E^{-1}$. After the simulation the pseudo particles are reweighted to a source spectrum $dN/dE \sim E^{-\alpha_s}$. Here we test $1 \leq \alpha_s \leq 3$ in steps of $\Delta\alpha_s = 0.1$. For the spatial distribution of CR sources we test two different scenarios:

1. The first scenario describes three point sources of CRs which are observed in gamma ray. We use the central source $J1745-290$ also called SgrA* , the pulsar $J1746-285$ and the super nova remnant $G0.9+0.1$. The contribution of the single sources to the total CR injection power is based on the results from [7].

2. In the second scenario CRs are injected homogeneously in the entire simulation volume. This corresponds to a population of "old" CRs, which have been accelerated outside the CMZ and diffused in before. In this scenario the injection spectrum should be closer to the observed spectrum at Earth $\sim E^{-2.7}$ than the prediction from diffusive shock acceleration $\sim E^{-2}$.

3.3 Simulation volume and boundary conditions

We chose the simulation volume to be a box of size $200 \times 400 \times 120\,\mathrm{pc}^3$, assuming the x-axis along the Sun-GC line, the y-axis in longitudinal, and the z-axis in the latitudinal direction. All CR candidates reaching the edge of the simulation volume are lost to the galaxy, and taken out of the simulation. Also a minimal energy for the CRs of 1 TeV is used. For this reason only gamma rays with energies higher than 100 GeV can be analysed. We allow for a maximal propagation time of $T_{\mathrm{max}} = 500\,\mathrm{kpc}/c$. This time has to be chosen long enough that nearly all particles can leave the volume before. In general the simulations with higher anisotropy of the diffusion tensor (lower values of ϵ) lead to higher residence times of CRs. In Fig. 2 the fraction of particles left in the simulation volume after a certain propagation time T is shown. It can be seen that more than 99.9% of the particles leave the simulation volume in less than $T = 100\,\mathrm{kpc}/c$. Secondary gamma rays produced in the simulation are directly written out. At this point no absorption is considered.

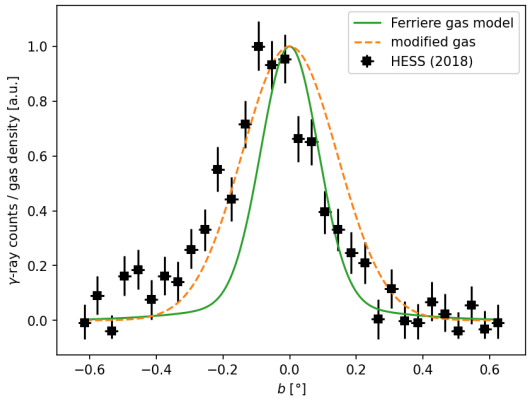

Figure 1: Latitudinal profile of the gamma rays (black, squares) and the gas distribution (green solid) from [1] and the modified version (dashed orange) assuming $H = 30$ pc.

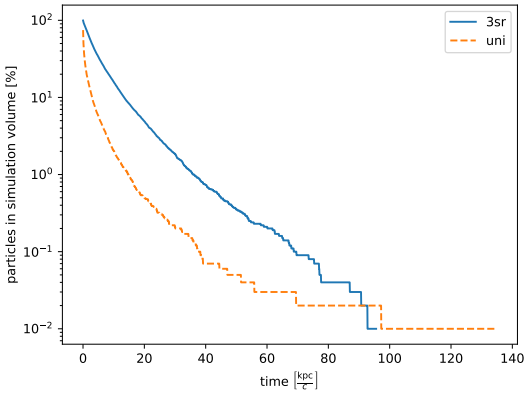

Figure 2: Fraction of particles left in the simulation volume. This simulation is done for $N = 10^4$ particles assuming $\epsilon = 0.001$.

4. Results

4.1 Spatial profiles of gamma ray emission

In [7] the spatial distribution of gamma rays along the longitudinal and latitudinal axis is reported. To compare our simulation with these profile we calculate histograms of the produced gamma rays with a binning of $\Delta l = 0.016°$ and $\Delta b = 0.01°$. The profiles are integrated over latitude $|b| \leq 0.3°$ and longitude $|l| \leq 0.5°$, respectively. This is chosen to match the integration used in [7]. After the binning, a Gaussian smearing with the resolution of the *H.E.S.S.* point spread function (PSF), $\sigma = 0.077°$, is performed. The latitudinal profile is used to normalise the simulations to match the data point of the *H.E.S.S.* observation at $b = -0.054°$, which is the middle of the peak of the latitudinal profile.

The observed and simulated profiles are shown in Fig. 3. The latitudinal profile follows for both injection scenarios, point sources (green circle) and homogeneous distribution (purple diamond), a Gauß-like shape. With increasing perpendicular diffusion (higher values of ϵ) the width of the disc becomes larger. No model reproduces the slight shift of the peak of the distribution to negative latitudes observed in the data. This is expected as the assumed gas distribution is symmetric around $z = 0$. This may be a hint that a better knowledge of the gas distribution is needed.

In the longitudinal profiles (left column) more differences between the spatial sources distributions and anisotropies of the diffusion tensor are visible. The point source injection (upper row) shows a much more peaked structure around $l = 0°$ and $l = 0.7°$. This is caused by an increased confinement of CRs in the magnetic field in the central 10 pc around SgrA* and in the molecular cloud SgrB2. Both locations are directly at the injection point or close to it. With increased perpendicular diffusion the peaks are spread out, as the escape of CRs becomes easier. This leads to a decreased residence time and a lower gamma ray production. In the less anisotropic cases with $\epsilon \geq 0.1$ a third peak around $l = 0.9°$ becomes visible. This is the injection point of the SNR $G0.9+01$. Also the homogeneous injection shows a peaked structure around the two points of high magnetic fields, although a more diffuse large scale emission can be seen. Compared to the point

source injection the peak at $l = 0.7°$ is much more pronounced and clearly overshoots the data. In the case of fully isotropic diffusion ($\epsilon = 1$) the distribution of gamma rays is flat for positive latitudes. Only at $l < 0°$ a decrease due to the vanishing density distribution can be seen.

To estimate the agreement of the simulated profiles with the data, the reduced χ^2 is calculated as

$$\chi^2_{\text{red}} = \frac{1}{n-1} \sum_{i=1}^{n} \frac{\left(c_i^{(\text{obs})} - c_i^{(\text{sim})}\right)^2}{\sigma_i^2}, \tag{3}$$

where c_i is the observed or calculated counts in the i-th bin and σ_i is the observation error. The result can be seen in Fig. 4. In general the χ^2 for the latitude (circles) is smaller compared to the longitudinal profiles (diamond). In both spatial source profiles the isotropic diffusion ($\epsilon = 1$) leads to the minimal χ^2, although the difference for $\epsilon \geq 0.1$ are quite small. In the longitudinal profile the best anisotropy parameter depends on the source distribution. In the case of the point source injection the isotropic diffusion is preferred. For the uniform injection a strong parallel diffusion with $\epsilon = 0.01$ leads to the best agreement with the data.

4.2 Spectral energy distribution

The second observable of the diffuse gamma ray emission in the CMZ is the spectral energy distribution (SED). Here, we analyse the impact of the CR injection spectrum. We test a power law injection $\frac{\mathrm{d}N}{\mathrm{d}E}\big|_{\mathrm{s}} \sim E^{-\alpha_s}$ with a spectral index α_s between 1 and 3 in steps of $\Delta\alpha_s = 0.1$. All gamma rays in a ring centred at SgrA* with a projected distance $0.15° \leq r \leq 0.45°$ are used to calculate the SED. The normalisation is chosen to match the observed data by *H.E.S.S.* [7] at $\sim$ 1 TeV. The calculated spectrum is fitted with a power law with exponential cut-off

$$\frac{\mathrm{d}N}{\mathrm{d}E} = \Phi_0 \left(\frac{E}{1\,\text{TeV}}\right)^{-\alpha} \exp\left\{-\frac{E}{E_c}\right\}, \tag{4}$$

where Φ_0 is the normalisation of the fit, α is the power law slope and E_c is the cut off energy. In Fig. 5 the observed spectrum by HESS and three different example spectra are shown. Here the point source injection and an intermediate anisotropy $\epsilon = 0.1$ is used.

To estimate the agreement of the fit with the observed data, the χ^2 is calculated by using eq. 3 and replacing c_i by the observed or simulated flux in the i-th bin. The result is plotted in Fig. 6. Both spatial source distribution and all anisotropies follow the same behaviour. All curves have a minimum at $\alpha_s = 2.1 \pm 0.1$ and a quick rise at softer injection spectra. Both source distribution have the best agreement of the simulated SED with the data for the anisotropy of $\epsilon = 0.01$ and an injection slope of $\alpha_s = 2.1$. The parameter for the best fit are given in table 1. While these values for the injection spectrum are reasonable for the point sources in the GC region, the explanation of an old CR population accelerated outside of the CMZ and diffused in would require a steeper spectrum.

5. Conclusion

The choice of the anisotropy of the diffusion tensor has a strong impact on the resulting distributions of gamma rays from the Galactic Centre. Our fits for the spatial distribution prefers a

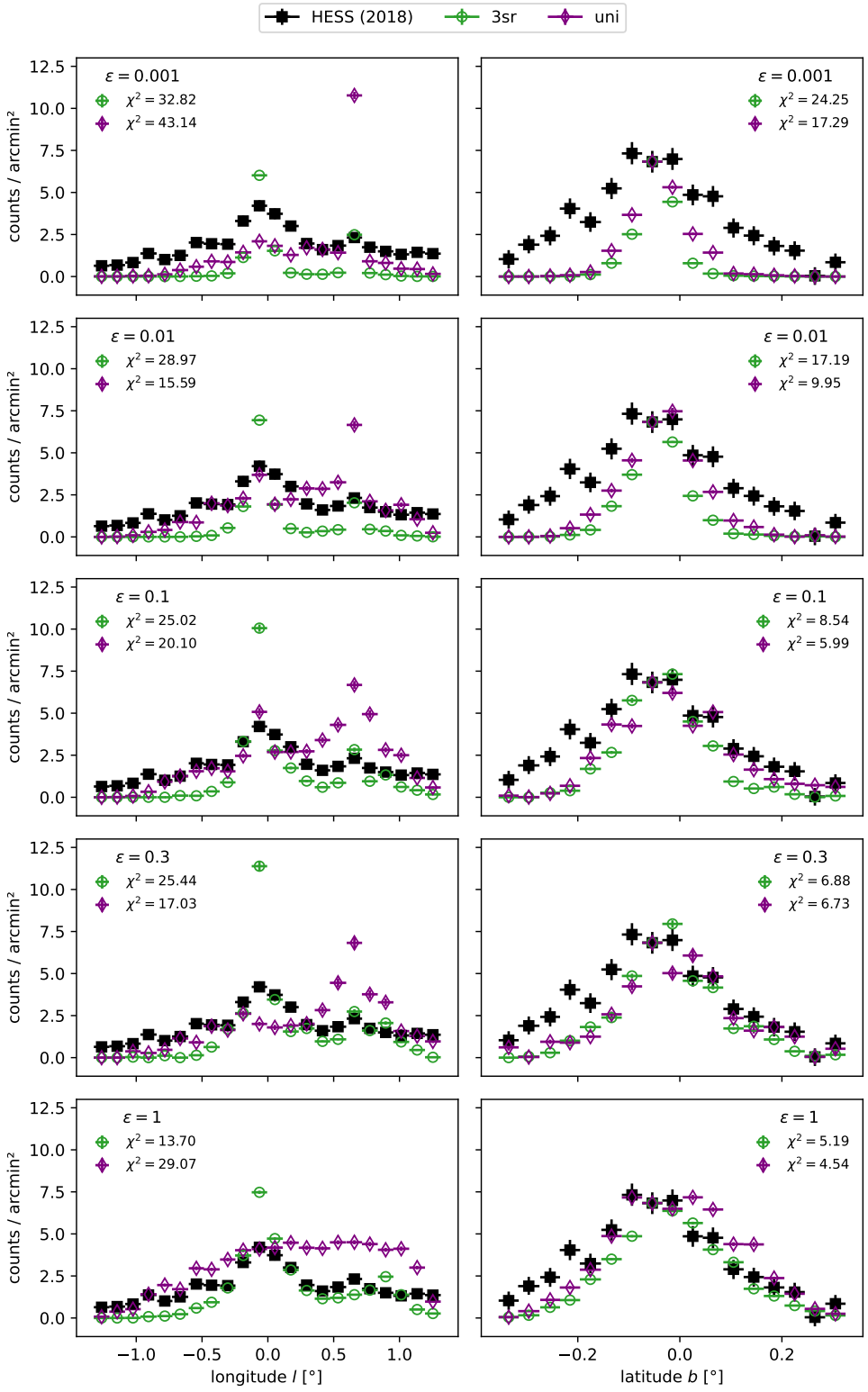

Figure 3: Spatial distribution of gamma rays for the point source injection (green circle) and the uniform injection (purple diamond). The profiles are given for the longitude (left column) and the latitude (right column). The rows indicate the effect of the different anisotropy of the diffusion tensor.

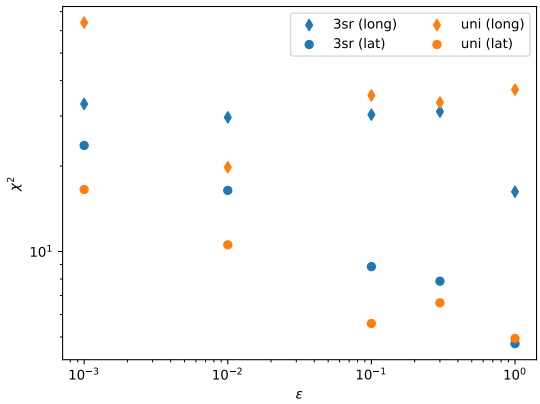

Figure 4: Calculated χ^2 value to estimate the agreement between the calculated countprofiles (see Fig. 3) and the data.

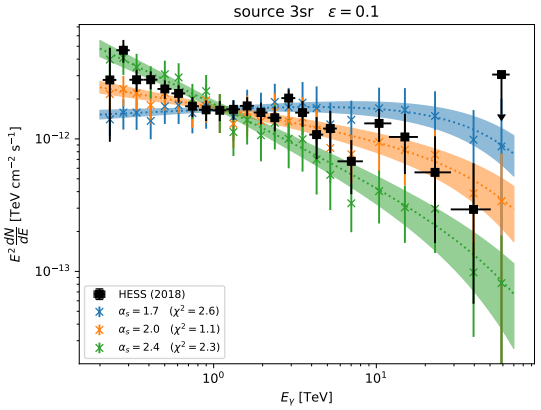

Figure 5: Energy weighted spectrum of the diffuse gamma ray flux. The crosses show the simulations for point source injection and the anisotropy parameter $\epsilon = 0.1$. The color indicates different injection indices and the fit following eq. 4.

setup			fit			
source	ϵ	α_s	$\log_{10}\left(\Phi_0[\mathrm{TeV\,cm^{-2}\,s^{-1}}]\right)$	α	E_c [TeV]	χ^2_{red}
3sr	0.01	2.1	-11.733 ± 0.011	2.268 ± 0.024	71 ± 12	0.79
uni	0.01	2.1	-11.705 ± 0.014	2.24 ± 0.03	62 ± 12	0.76

Table 1: Best fit parameter for the minimal χ^2 shown in Fig. 6. We note that the normalisation of the simulated spectrum is chosen to match the HESS data point at 1 TeV. Therefore, no significant change for the fit normalisation is expected.

injection by point sources inside of the CMZ and an isotropic diffusion. This would require an nearly fully turbulent environment, which has not been observed so far. The shift of the latitudinal profile the $b \leq 0°$ can not be reproduced and shows that an adjustment of the gas distribution is needed. On the other way the fits to the SED prefer a quite strong parallel diffusion with $\epsilon = \kappa_\perp/\kappa_\parallel = 0.01$, although we have to note that the difference to the less anisotropic cases are not so strong for the spectrum. In general a more detailed knowledge of the 3D gas distribution and the magnetic field is needed to allow a better modelling of the VHE emission in the CMZ.

acknowledgements We acknowledge the support from the DFG via the Collaborative Research Center SFB1491 *Cosmic Interacting Matters - From Source to Signal* (project no. 445052434).

References

[1] K. Ferrière, W. Gillard, P. Jean, *A&A*, **467**, 611 (2007).

[2] Y. Sofue *MNRAS*, **516**, 3911-3923 (2022).

[3] M. Di Mauro *Phys.Rev.D*, **103**, 063023 (2021).

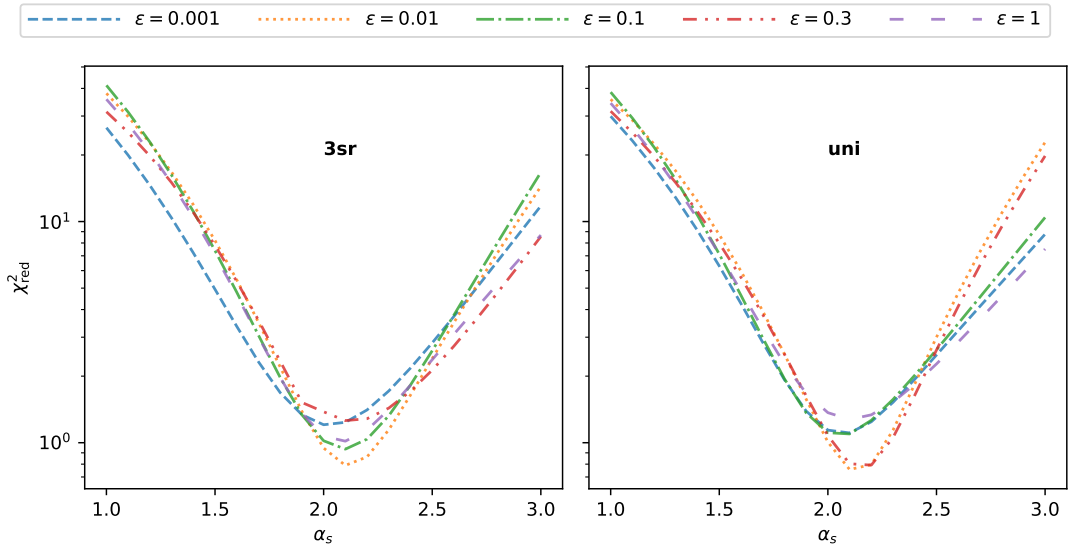

Figure 6: Calculated χ^2 for the agreement of the fitted SED to the data.

[4] I. Cholis, Y-M. Zhong, D. Samuel, *et al.*, *Phys.Rev.D*, **108**, 103023 (2022).

[5] M. Pohl, O. Macias, P. Coleman, *et al.*, *ApJ*, **929**, 136 (2022).

[6] HESS Collaboration, *Nature*, **531**, 476-479 (2016).

[7] HESS Collaboration, *A&A*, **612**, A9 (2018).

[8] A. Scherer, J. Cuandra and F.E. Bauer, *A&A*, **659**, A105 (2022).

[9] J.R. Jokipii, *ApJ*, **146**, 480 (1966).

[10] M.S. Potgieter, *Space Sci Rev*, **176**, 165-176 (2013).

[11] P. Reichherzer, J. Becker Tjus, E. G. Zweibel *et al.*, *MNRAS*, **498**, 5051 (2020).

[12] P. Reichherzer, J. Becker Tjus, E. G. Zweibel *et al.*, *MNRAS*, **514**, 2658 (2022).

[13] P. Reichherzer, L. Merten, J. Dörner *et al.*, *SN Appl. Sci.*, **4**, 15 (2022).

[14] F. Effenberger, H. Fichtner, K. Scherer *et al.*, *A&A*, **547**, A120 (2012).

[15] L. Merten, C. Bustard, E.G. Zweibel *et al.*, *ApJ*, **859**, 63 (2018).

[16] M. Guenduez, J. Becker Tjus, K. Ferrière, *et al.*, *A&A*, **644**, A71 (2020).

[17] R. Alves Batista, J. Becker Tjus, J. Dörner, *et al.*, *JCAP*, **09**, 035 (2022).

[18] S.R. Kelner, F.A. Aharonian, and V.V. Bugayov, *Phys. Rev. D*, **74**, 034018 (2006).

[19] M.R. Hoerbe, P.J. Morris, G.Cotter, *et al.*, *MNRAS*, **496**, 3, 2885-2901 (2020).

[20] J. Becker Tjus, L. Merten, *Physics Reports*, **872**, 1-98 (2020).